

# Modeling the columnar-to-equiaxed transition with a three-phase Eulerian approach

Andreas Ludwig, Menghuai Wu\*

*Christian-Doppler-Lab for Multiphase Modeling of Metallurgical Processes, Department of Metallurgy,  
University of Leoben, Franz-Josef-Str. 18, A-8700 Leoben, Austria*

Received in revised form 1 July 2005

## Abstract

A three-phase Eulerian approach is developed to model the columnar-to-equiaxed transition (CET) during solidification. The three phases are the parent melt, the solidifying columnar dendrites and the solidifying equiaxed grains. They are considered as spatially interpenetrating and interacting continua. We solve the conservation equations of mass, momentum, species and enthalpy for all three phases. Additionally we define and solve an additional transport equation for the number density of equiaxed grains which also accounts for grain nucleation. Diffusion controlled growth for both columnar and equiaxed phases, drag forces, species partitioning at the solid/liquid interface, heat of fusion, etc. are taken into account with the corresponding closure laws. A binary “steel” (Fe–0.34 wt.% C) ingot casting as benchmark was simulated to demonstrate the model potentials. Preliminary results of the mixed columnar and equiaxed solidification including the motion of the columnar tip front, the occurrence of the CET, the formation of macrosegregations, and the resulting melt convection and grain sedimentation and their influence on the final macroscopic phase distribution are presented.

© 2005 Elsevier B.V. All rights reserved.

*Keywords:* Solidification; Multiphase; Columnar-equiaxed transition; Macrosegregation; Sedimentation; Convection

## 1. Introduction

In recent years, the authors developed two two-phase models, one for equiaxed solidification [1–4] and another for hypermonotectic solidification [5–7]. Both models are based on an Eulerian–Eulerian approach. This paper reports about the extension of the two-phase equiaxed solidification model to a three-phase model for a mixed columnar and equiaxed solidification with consideration of the so-called columnar-to-equiaxed transition (CET).

With an additional (columnar) phase, one more set of conservation equations for mass, enthalpy and species must be solved. No additional momentum equation is solved, as the columnar phase is considered to be stationary. The most challenging point is the appropriate definition of the closure laws for the phase exchanges and interactions: e.g. the competitive growth of both solid phases, and the mechanical interaction between them. The equiaxed phase which is allowed to nucleate

everywhere in bulk melt, grows and moves freely. The stationary columnar phase is regarded to start from the mold wall and grows thus preferentially along the heat flow direction. During solidification, both phases grow competitively. A so-called columnar-to-equiaxed transition (CET) occurs at the end of solidification when the growing columnar dendrite tips are blocked by equiaxed grains. Early studies reported two ‘blocking’ mechanisms: one is by ‘mechanical blocking’ when the local volume fraction of equiaxed grain envelopes exceeds a certain limit [8], the other is by ‘soft-blocking’ when the local constitutional undercooling disappears [9,10]. The presented three-phase model tracks the columnar tip front explicitly, and includes both of the above-mentioned CET mechanisms. However, in our work the impact of the melt convection and equiaxed grain transport on the occurrence of CET is also considered.

## 2. Model

### 2.1. General assumptions

- (1) Three phases are defined: primary liquid phase (l), equiaxed phase (e), and columnar phase (c). The corresponding phase

\* Corresponding author. Tel.: +43 3842 4022223; fax: +43 3842 4022202.  
E-mail address: menghuai.wu@notes.unileoben.ac.at (M. Wu).

volume fractions  $f_l$ ,  $f_e$  and  $f_c$  are subject to  $f_l + f_e + f_c = 1$ . Both, the primary liquid phase and the equiaxed phase are allowed to move. The columnar phase is assumed to stick to the wall, and solidify from the wall towards the bulk melt along the heat flow direction. No momentum equation for the columnar phase is solved.

- (2) Ideal morphologies for both solid phases are assumed: spherical for the equiaxed (globular) grains and cylindrical for the columnar (cellular) primary dendrites.
- (3) The grain size of the equiaxed grains is explicitly calculated, while a constant value for the primary dendrite arm spacing is assumed for the columnar phase.
- (4) The Boussinesq approach is used to model thermo-solutal convection, grain sedimentation and sedimentation-induced melt convection. The volume shrinkage is ignored.
- (5) Grains created or brought into the mold during filling, and fragmentation (or segmentation) of the dendrites are not modeled.

## 2.2. Nucleation of equiaxed grains and grain transport

The number density of equiaxed grains ( $m^{-3}$ ),  $n$ , is calculated with

$$\frac{\partial}{\partial t} n + \nabla \cdot (\vec{u}_e n) = N_e \quad (1)$$

Here,  $\vec{u}_e$  is the (volume averaged) velocity of the equiaxed phase. The nucleation rate ( $m^{-3} s^{-1}$ ),  $N_e$ , is modeled with a three-parameter heterogeneous nucleation law [1,2].

## 2.3. Mass conservation and grain growth kinetics

Mass conservation equations are

$$\frac{\partial}{\partial t} (f_l \rho_l) + \nabla \cdot (f_l \rho_l \vec{u}_l) = M_{el} + M_{cl}, \quad (2)$$

$$\frac{\partial}{\partial t} (f_e \rho_e) + \nabla \cdot (f_e \rho_e \vec{u}_e) = M_{le} + M_{ce}, \quad (3)$$

$$\frac{\partial}{\partial t} (f_c \rho_c) + \nabla \cdot (f_c \rho_c \vec{u}_c) = M_{lc} + M_{ec}, \quad (4)$$

where  $\rho_l$ ,  $\rho_e$ ,  $\rho_c$ , are the densities and  $\vec{u}_l$ ,  $\vec{u}_e$ ,  $\vec{u}_c$  the velocities of the different phases. The source terms  $M_{lc}$  ( $= -M_{cl}$ ) is the mass transfer rate ( $kg/m^3/s$ ) from liquid to columnar phase, and  $M_{le}$  ( $= -M_{ce}$ ) from liquid to equiaxed phase by solidification (positive) or melting (negative), and  $M_{ce}$  ( $= -M_{ec}$ ) from columnar to equiaxed phase by the mechanism of fragmentation (positive) or by attaching (negative). The fragmentation is ignored, so we chose  $M_{ce} = 0$ .

Diffusion controlled grain growth kinetics at the micro scale is considered. For equiaxed solidification an ideal spherical morphology is considered so that the grain growth velocity in the radius direction can be solved analytically [11]

$$v_{R_e} = \frac{dR_e}{dt} = \frac{D_l}{R_e} \frac{c_1^* - c_1}{c_1^* - c_s^*} = \frac{D_l}{R_e(1-k)} \left( 1 - \frac{c_1}{c_1^*} \right) \quad (5)$$

Here,  $c_1^*$  and  $c_s^*$  ( $c_s^* = kc_1^*$ ) are the equilibrium concentrations adjacent to the solid/liquid interface, and from the phase diagram  $c_1^* = (T - T_f)/m$  yields.  $D_l$  is the diffusion coefficient in the liquid and  $R_e = d_e/2$  the radius of the grain. With Eq. (5), we can define the volume averaged mass transfer rate for globular equiaxed solidification by considering the total surface area of the spherical grains and the influence of pinging by an Avrami-factor  $f_l$

$$M_{le} = v_{R_e} (n\pi d_e^2) \rho_e f_l \quad (6)$$

For columnar solidification two different cases are distinguished: (i) tip regions and (ii) growing columnar trunks behind the tip region. We trace the tip front of the columnar grains by a method described in Section 2.8. For the volume elements which have already been pasted by the tip front a diffusion controlled growth model around cylindrical dendrite trunks is used. With the similar analytical method of [11], the growth velocity in radial direction of such a cylindrical trunk is approximated by

$$v_{R_c} = \frac{dR_c}{dt} = \frac{D_l}{R_c} \frac{c_1^* - c_1}{c_1^* - c_s^*} \ln^{-1} \left( \frac{R_f}{R_c} \right), \quad (7)$$

where now  $R_c = d_c/2$  is the average radius of a cylindrical dendrite trunk and  $R_f = \lambda_1/2$  is half of the primary dendrite spacing  $\lambda_1$ . So we can define the volume averaged mass transfer rate for those volume elements by considering the total surface area of columnar dendrite trunks per volume  $S_A = \pi d_c/\lambda_1^2$  and an Avrami-factor  $f_l$

$$M_{lc} = v_{R_c} \left( \frac{\pi d_c}{\lambda_1^2} \right) \rho_c f_l \quad (8)$$

For the elements containing the growing columnar tips, the mass transfer rate  $M_{lc}$  for columnar solidification is written by considering both the tip growth velocity,  $v_{tip}$ , and radial growth velocity,  $v_{R_c}$

$$M_{lc} = v_{R_c} n_c (\pi d_c l) \rho_l f_l + v_{tip} n_c (\pi R_{tip}^2) \rho_l f_l \quad (9)$$

The first term on the left hand side of Eq. (9) denotes the mass transfer rate due to the growth in radial direction and the second term that of the growth in tip direction.  $n_c = 4f_c/(\pi d_c^2 l)$  is the number density of the columnar trunks. The dendrite tip velocity  $v_{tip}$  and the tip radius  $R_{tip}$  are calculated according to [11,12].

## 2.4. Momentum conservation

The momentum equations for the parent melt and the moving equiaxed phase are

$$\begin{aligned} \frac{\partial}{\partial t} (f_l \rho_l \vec{u}_l) + \nabla \cdot (f_l \rho_l \vec{u}_l \otimes \vec{u}_l) \\ = -f_l \nabla p + \nabla \cdot \vec{\tau}_l + \vec{F}_{Bl} + \vec{U}_{cl} + \vec{U}_{el}, \end{aligned} \quad (10)$$

$$\begin{aligned} \frac{\partial}{\partial t} (f_e \rho_e \vec{u}_e) + \nabla \cdot (f_e \rho_e \vec{u}_e \otimes \vec{u}_e) \\ = -f_e \nabla p + \nabla \cdot \vec{\tau}_e + \vec{F}_{Be} + \vec{U}_{le} + \vec{U}_{ce}, \end{aligned} \quad (11)$$

where  $\bar{\tau}_l$  and  $\bar{\tau}_e$  are the stress–strain tensors. With the Boussinesq approximation, the thermal-solutal buoyancy force  $\bar{F}_{Bl}$  acting on the liquid and the buoyancy force  $\bar{F}_{Be}$  acting on the free moving equiaxed grains are applied [4]. Each of the momentum exchange terms  $\bar{U}_{le}$ ,  $\bar{U}_{lc}$  and  $\bar{U}_{ce}$  includes two parts: the part due to phase transformation and the part due to drag force, for example,  $\bar{U}_{le} = \bar{U}_{le}^p + \bar{U}_{le}^d$  and  $\bar{U}_{lc} = \bar{U}_{lc}^p + \bar{U}_{lc}^d$ . Details to treat these momentum exchange term between the liquid phase and the equiaxed phases are described in [1,2]. The same idea is used for the momentum exchange between the liquid and the columnar phase. However, we calculated the liquid-columnar drag force by considering a mushy zone permeability as proposed in [13]. For the momentum exchange between the columnar and the equiaxed phase a simple approach is used. We assumed that when the local volume fraction of the columnar phase is more than a critical value of  $f_c^{\text{free}} = 0.2$ , an infinite drag force coefficient between both solid phases applies and thus the equiaxed grains are captured. When the volume fraction of the columnar phase is smaller than this critical value, no drag force between both solid phases exists and thus the motion of the equiaxed grains is not affected by the columnar front. The choice of the critical value for  $f_c^{\text{free}} = 0.2$  is here arbitrary. Therefore, further parameter study on the influence of this value on the final result is necessary.

### 2.5. Species conservations

The volume averaged concentration  $c_l$  in the liquid phase,  $c_e$  in the equiaxed phase and  $c_c$  in the columnar phase are obtained by solving the species concentration equations:

$$\begin{aligned} \frac{\partial}{\partial t}(f_l \rho_l c_l) + \nabla \cdot (f_l \rho_l \bar{u}_l c_l) \\ = \nabla \cdot (f_l \rho_l D_l \nabla c_l) + C_{cl} + C_{el}, \end{aligned} \quad (12)$$

$$\begin{aligned} \frac{\partial}{\partial t}(f_e \rho_e c_e) + \nabla \cdot (f_e \rho_e \bar{u}_e c_e) \\ = \nabla \cdot (f_e \rho_e D_e \nabla c_e) + C_{le} + C_{ce}, \end{aligned} \quad (13)$$

$$\begin{aligned} \frac{\partial}{\partial t}(f_c \rho_c c_c) + \nabla \cdot (f_c \rho_c \bar{u}_c c_c) \\ = \nabla \cdot (f_c \rho_c D_c \nabla c_c) + C_{lc} + C_{cc}, \end{aligned} \quad (14)$$

where  $D_l$ ,  $D_e$ ,  $D_c$  are the diffusion coefficients. The diffusive species exchange at the phase interface is ignored, but the species partitioning at the phase interface during solidification (and melting) is taken into account [1,2]. As we ignore any phase exchange between equiaxed and columnar phases, we set  $C_{ce} \equiv 0$ .

### 2.6. Enthalpy conservation

We solve the enthalpy conservation equation for each phase

$$\begin{aligned} \frac{\partial}{\partial t}(f_l \rho_l h_l) + \nabla \cdot (f_l \rho_l \bar{u}_l h_l) \\ = \nabla \cdot (f_l k_l \nabla \cdot T_l) + Q_{cl} + Q_{el}, \end{aligned} \quad (15)$$

$$\begin{aligned} \frac{\partial}{\partial t}(f_e \rho_e h_e) + \nabla \cdot (f_e \rho_e \bar{u}_e h_e) \\ = \nabla \cdot (f_e k_e \nabla \cdot T_e) + Q_{le} + Q_{ce}, \end{aligned} \quad (16)$$

$$\begin{aligned} \frac{\partial}{\partial t}(f_c \rho_c h_c) + \nabla \cdot (f_c \rho_c \bar{u}_c h_c) \\ = \nabla \cdot (f_c k_c \nabla \cdot T_c) + Q_{lc} + Q_{ec}, \end{aligned} \quad (17)$$

where the enthalpies are defined via  $h_l = \int_{T_{\text{ref}}}^{T_l} c_{p(l)} dT + h_l^{\text{ref}}$  and  $h_e = h_c = \int_{T_{\text{ref}}}^{T_e} c_{p(s)} dT + h_e^{\text{ref}}$  with specific heat of the liquid  $c_{p(l)}$  and the solid phase  $c_{p(s)}$ .  $T_{\text{ref}}$  and  $h_e^{\text{ref}}$  are defined so that the enthalpy difference between liquid and any solid,  $h_l - h_e$  and  $h_l - h_c$ , is equal to the latent heat of fusion. Further details to treat the latent heat can be found in previous publications [1,2]. By solving Eqs. (15)–(17), three different temperatures are obtained,  $T_l$ ,  $T_e$  and  $T_c$ . The thermal equilibrium condition ( $T_l \approx T_e \approx T_c$ ) is satisfied by applying a quite large volumetric heat transfer coefficient of  $10^8$  ( $\text{W m}^{-3} \text{K}^{-1}$ ) between the phases.

### 2.7. Auxiliary quantities

A mixture concentration for the description of macrosegregations,  $c_{\text{mix}}$ , is defined by

$$c_{\text{mix}} = \frac{c_l \rho_l f_l + c_e \rho_e f_e + c_c \rho_c f_c}{\rho_l f_l + \rho_e f_e + \rho_c f_c}. \quad (18)$$

The average diameter of the equiaxed grains,  $d_e$ , is calculated from the following relation

$$f_e = n \frac{4\pi}{3} \left( \frac{d_e}{2} \right)^3. \quad (19)$$

The average diameter of the columnar dendrite trunks,  $d_c$ , is calculated by relating the cross section area of a single columnar trunk,  $\pi(d_c/2)^2$ , to the maximal available area of each trunk when the dendrites are ranked in hexagon. Thus, we get

$$f_c = \frac{3}{4} \frac{d_c^2}{\lambda_1^2}. \quad (20)$$

In the case the dendrites are ranked in square, the prefactor of Eq. (20) would be  $\pi/4$  instead of  $3/4$ . In this paper, the average dendrite arms spacing,  $\lambda_1$ , is assumed to be constant and given. For the results presented in this paper we took  $\lambda_1 = 1$  mm.

### 2.8. Columnar tip front tracking and tip front ‘blocking’ mechanism

The columnar tip front tracking is based on the assumption that columnar dendrite trunks grow from the wall into the bulk melt. However, no growth-preferred crystalline orientation is considered.

- (1) Each control volume is indexed with a columnar status marker,  $i_c$ , which indicates whether a control volume contains the columnar tip front ( $i_c = 1$ ); columnar dendrite

- trunks ( $i_c = 2$ ); or no trunks or tips ( $i_c = 0$ ). All control volumes are initialized with  $i_c = 0$ , except the boundary (wall) elements where  $i_c = 1$ .
- (2) For each control volume an “equivalence” cylinder is considered with a radius of  $l_{\text{ref}}$  and a height of  $l_{\text{ref}}$ . The volume of the cylinder is chosen to be equal to that of the corresponding control volume:  $\pi l_{\text{ref}}^3 = \Delta V$ . As no preferred crystal growth orientation is predefined, the “equivalence” cylinder is thought to be orientated parallel to the local heat flow direction.
  - (3) The columnar front grows parallel to the “equivalence” cylinder with a growth velocity,  $v_{\text{tip}}$ , which is determined from the LGT model [11,12]. The actual position of the front is tracked by evaluating the integral  $l = \int_t v_{\text{tip}} dt$ , starting as soon as the front first enters the control volume.
  - (4) For  $l > l_{\text{ref}}$  the columnar tip front has grown out of the “equivalence” cylinder. In this case all neighboring control volumes which are still “empty” ( $i_c = 0$ ) will be “reached” by the front. Thus, the columnar status markers of these volumes are set to  $i_c = 1$ , whereas the marker of the considered volume is set to  $i_c = 2$ .
  - (5) A mass transfer from the liquid to the columnar phase is only considered for those control volumes  $i_c \neq 0$ .
  - (6) In order to model the ‘mechanical blocking’ mechanism by Hunt [8] the tip growth velocity is set to zero,  $v_{\text{tip}} \equiv 0$ , as soon as the local volume fraction of equiaxed,  $f_e$ , increases over the critical threshold of  $f_{e,\text{CET}} = 0.49$ . This event defines what is known in the literature as CET. The above described procedure for the CET automatically leads to the so-called ‘soft-blocking’ mechanism proposed by Martorano et al. [10], as  $v_{\text{tip}}$  vanishes when the local constitutional undercooling disappears.

## 2.9. Numerical implementation

The conservation equations are numerically solved with the control-volume based finite difference CFD software FLUENT 6.1. The closure laws are implemented as user defined functions. The FLUENT formulation is fully implicit, hence there is no stability criterion for the time step,  $\Delta t$ . However, the time steps used in practice impact on the accuracy of the calculation, thus the reliability of the numerical result. The  $\Delta t$  must be determined empirically by test simulations. For the benchmark simulation in Section 3 a time step of  $\Delta t = 10^{-4}$  s was used to start the simulation, and later change to  $10^{-3}$  s. For each time step, up to 60 iterations were necessarily to decrease the normalized residual of  $c_l$ ,  $c_e$ ,  $c_c$ ,  $f_e$ ,  $f_c$ ,  $\vec{u}_l$ ,  $\vec{u}_e$ ,  $p$  and  $n$  below the convergence limit of  $10^{-4}$ , and  $h_l$ ,  $h_e$ , and  $h_c$  below that of  $10^{-7}$ .

## 3. Benchmark

The solidification of a binary “steel” (Fe–0.34 wt.% C) ingot with a relatively small size (diameter: 66 mm, height: 170 mm) was simulated (see Fig. 1). An axis-symmetrical simulation is made. The grid used consists of 690 elements with a mean size of  $6 \text{ mm}^2$ . The ingot is filled instantaneously with temperature

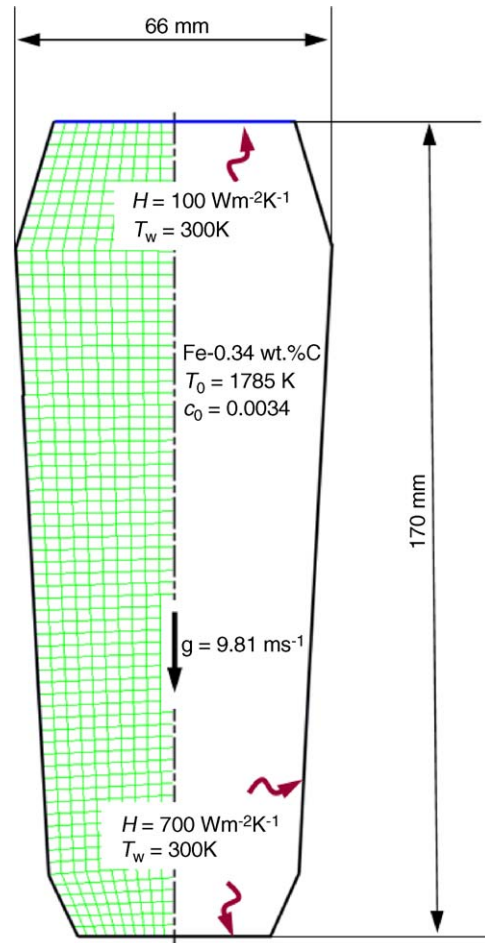


Fig. 1. Schematic of the simulated benchmark (average grid size  $2.5 \text{ mm} \times 2.5 \text{ mm}$ ).

of 1785 K. All properties and parameters used for the simulation are listed in Table 1 and Fig. 1.

Fig. 2 shows the solidification sequence of the ingot casting. Solidification starts as soon as the temperature drops down below liquidus (1782.3 K). At 5 s, the equiaxed grains start to sink, and induce melt convection. The melt is dragged by the sinking grains downwards along the wall and then rises again in the middle of the casting. Two symmetrical vortices form. In addition to the grain-sedimentation-induced melt convection, thermal and solute buoyancy also drives melt convection. The melt near the

Table 1  
Properties and parameters used in simulation

Thermal physical	Thermal dynamics	Process parameters
$c_{p(l)} = c_{p(s)} = 808.25 \text{ J kg}^{-1} \text{ K}^{-1}$	$k = 0.2894$	$n_{\text{max}} = 5 \times 10^9 \text{ m}^{-3}$
$D_l = 2 \times 10^{-8} \text{ m}^2 \text{ s}^{-1}$	$m = -8453.0 \text{ K}$	$\Delta T_N = 5 \text{ K}$
$D_e = D_c = 5.6 \times 10^{-10} \text{ m}^2 \text{ s}^{-1}$	$T_f = 1811 \text{ K}$	$\Delta T_\sigma = 2 \text{ K}$
$\Delta h_f = h_l^{\text{ref}} - h_e^{\text{ref}} = 256476 \text{ J kg}^{-1}$	$\Gamma = 2.9 \times 10^{-7} \text{ mK}$	
$k_l = k_e = k_c = 33.94 \text{ W m}^{-1} \text{ K}^{-1}$		
$\beta_T = 0.0002 \text{ K}^{-1}$		
$\beta_c = 0.011 \text{ wt.\%}^{-1}$		
$\rho_l = \rho_e = \rho_c = 7027 \text{ kg m}^{-3}$		
$\Delta \rho = 294 \text{ kg m}^{-3}$		

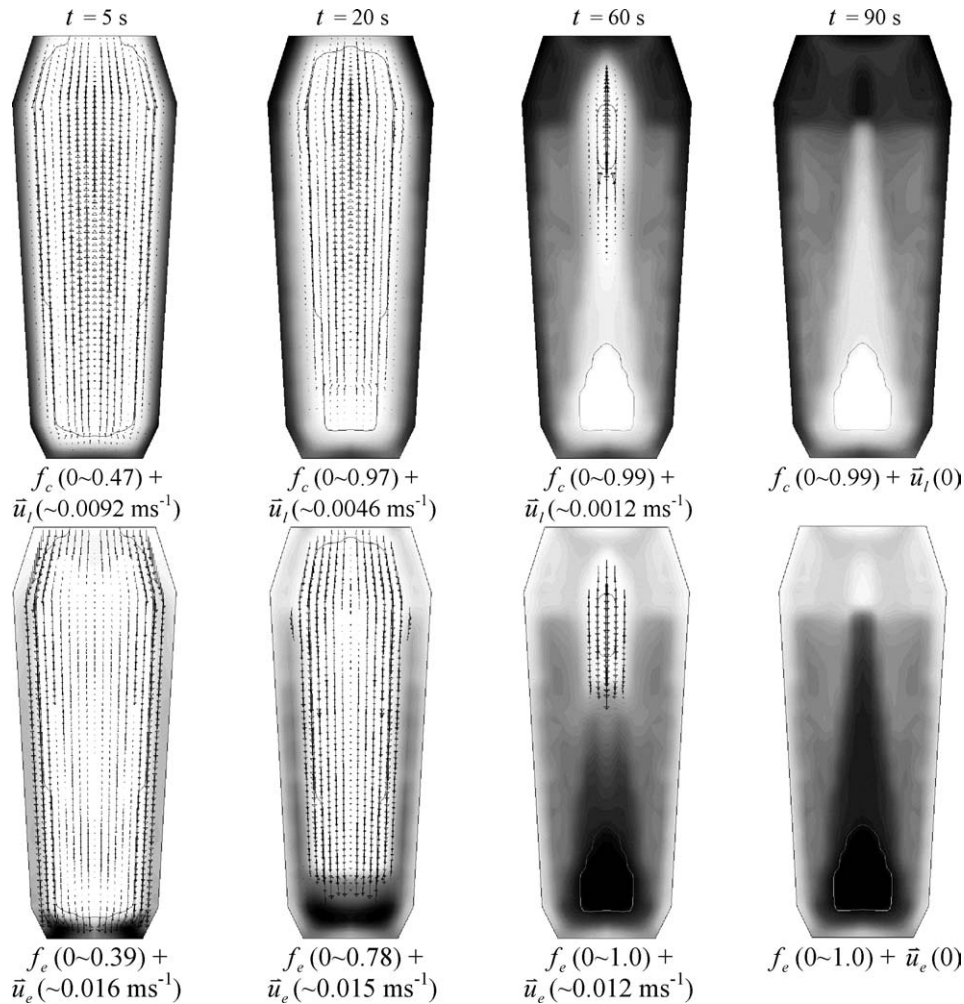


Fig. 2. Solidification sequences. Both  $f_c$  and  $f_e$  are shown with 60 gray levels. The maximum and minimum values of them are given. The arrows of both velocities are linearly scaled starting from zero to the maximum value. The columnar tip front with solid line overlaps the quantities  $f_c$  and  $f_e$ .

wall revealed a lower temperature and is thus heavier than the bulk melt ( $\beta_T > 0$ ) and enhance the flow. On the contrary, the effect of solute buoyancy is reverse compared with thermal buoyancy. The melt near the mold is enriched with solute, thus is less dense ( $\beta_c > 0$ ) and so tends to rise. From the flow pattern of Fig. 2, it becomes obvious that the joint effect of thermal buoyancy and grain-sedimentation-induced flow dominates the overall convection pattern. Sedimentation, of course, influences the distribution of equiaxed grains. The equiaxed grains sink down, and settle at the bottom region, where the volume fraction of the equiaxed phase reaches a quite high level, i.e. 39% at  $t = 5$  s.

In the course of further cooling, the volume fraction of the columnar phase at the mold wall increases. In addition, the equiaxed grains continue to nucleate, sink and grow. They settle and pile up in the lower region of the ingot. At  $t = 20$  s, the volume fraction of columnar phase near the wall reaches 97% and the volume fraction of equiaxed phase in the lower part of the ingot reaches 78%. In the mean time the columnar tip front moves inwards. As described in Section 2.4, it is assumed that the equiaxed grains can freely move until the volume fraction of

columnar dendrite trunks reaches 20%, when they are blocked and incorporated in the columnar front.

At  $t = 60$  s, the columnar tip front in the middle of the casting meets. Therefore, two closed columnar tip front lines are seen: one in the upper region where the solid fraction is still low, and a second in the lower part of the casting, where the solidification is nearly completed by equiaxed grains ( $f_e \geq 0.99$ ). Here the columnar tip front has already been ‘blocked’ by the presence of many equiaxed grains. The columnar tip front line in the upper part is still able to move.

At  $t = 90$  s the solidification of the whole casting is almost finished. The columnar tip front in the upper part of the casting has disappeared. However, in the lower part of the casting the columnar tip front still remains. This remaining columnar tip front line indicates the position of the CET. Within the CET line only equiaxed grains exist, while out of the line both columnar phase and equiaxed phases coexist.

The macrosegregation is shown in Fig. 3. A cone shaped negative segregation is predicted in the lower part of the ingot, where high sedimentation rate occurs. It is numerically ‘evidenced’ that the mechanism of the sedimentation of equiaxed

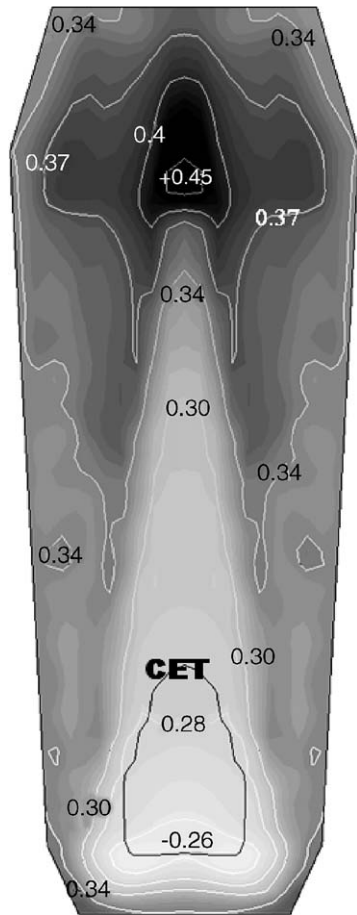


Fig. 3. Predicted macrosegregation  $c_{\text{mix}}$ . The quantity of  $c_{\text{mix}}$  is shown with both isolines and gray scale: light for negative segregation and dark for positive segregation. The values accompanying  $c_{\text{mix}}$  isolines are in unit of percentage. The CET (black line) is also drawn together with  $c_{\text{mix}}$ .

grains is responsible for the negative segregation. The solute poor equiaxed grains pile up at the bottom of the ingot, and the solute rich residual melt rises. The  $c_{\text{mix}}$  distribution profiles are approximately similar to the CET profile.

The positive segregation zone which forms at the top part of the ingot is mainly due to melt convection. The solute rich melt rises as the equiaxed grains sink. The solute redistribution in the melt is strongly dependent on the melt convection pattern. As shown in Fig. 2, two symmetrical melt vortices occur in the ingot. In the casting center the flow current transport solute rich melt from the bottom region towards the top. As the melt hits the casting top, it diverges into two side streams, resulting in a left- and a right-hand side region enriched with solute elements. Obviously, the positive segregated zones are not stationary during solidification, they move with the flow

current until the whole casting had solidified and the melt flow disappeared.

The modeling results described above reproduce the sense, which was described by Campbell [14] based on the understanding to classical experiments. The positive segregation at the top region of the ingot can be explained by the convection of the segregated melt in bulk region. This kind of positive segregation coincides with the early experimental results of Campbell [14] and Nakagawa and Momose [15]. Finally, it must be mentioned that channel segregations, which are frequently found in steel ingots, are not predicted with the recent model. The reason for that is that melting was not taken into account in this simulation and that the used numerical grid is too coarse.

#### 4. Summary

A three-phase Eulerian solidification model is developed, and preliminarily used to simulate a reduced ‘steel’ ingot. The result has shown the potential of the mixed columnar and equiaxed solidification including CET. The simulated solidification sequence, the sedimentation of the equiaxed grains, the movement of the columnar tip front and the final macroscopic phase distribution fit to the widely accepted explanations of experimental findings, as summarized by Campbell [14]. However, no quantitative evaluation was made yet. We rather suggest that further comprehensive parameter studies are necessary in order to analyze the importance of the different modeling assumptions.

#### References

- [1] A. Ludwig, M. Wu, *Metall. Mater. Trans. A* 33 (2002) 3673–3683.
- [2] M. Wu, A. Ludwig, A. Bührig-Polaczek, P.R. Sahm, *Inter. J. Heat Mass Transfer* 46 (2003) 2819–2832.
- [3] M. Wu, A. Ludwig, *Adv. Eng. Mater.* 5 (2003) 62–66.
- [4] M. Wu, A. Ludwig, J. Luo, *Mater. Sci. Forum* 475–479 (2005) 2725–2730.
- [5] M. Wu, A. Ludwig, L. Ratke, *Model. Simul. Mater. Sci. Eng.* 11 (2003) 755–769.
- [6] M. Wu, A. Ludwig, L. Ratke, *Metall. Mater. Trans. A* 34 (2003) 3009–3019.
- [7] A. Ludwig, M. Wu, M. Abodano, L. Ratke, *Mater. Sci. Forum* 508–509 (2006) 193–198.
- [8] J.D. Hunt, *Mater. Sci. Eng.* 65 (1984) 75–83.
- [9] C.Y. Wang, C. Beckermann, *Metall. Mater. Trans. A* 25 (1994) 1081–1093.
- [10] M. Martorano, C. Beckermann, Ch.-A. Gandin, *Metall. Mater. Trans. A* 34 (2003) 1657–1674.
- [11] W. Kurz, D.J. Fisher, *Fundamentals of Solidification*, Trans Tech Publications, Aedemansdorf, Switzerland, 1989.
- [12] J. Lipton, M.E. Glicksman, W. Kurz, *Mater. Sci. Eng.* 65 (1984) 57–63.
- [13] J.P. Gu, C. Beckermann, *Metall. Trans. A* 30 (1999) 1357–1366.
- [14] J. Campbell, *Castings*, Butterworth Heinemann Ltd., Oxford, 1991.
- [15] Y. Nakagawa, A. Momose, *Tetsu-to-Hagane* 53 (1967) 1477–1508.